Geomorphology 338 (2019) 16–26

Contents lists available at ScienceDirect

Geomorphology

journal homepage: www.elsevier.com/locate/geomorph

Global open-access DEM performances in Earth's most rugged region High Mountain Asia: A multi-level assessment

Kai Liu [a], Chunqiao Song [a,*], Linghong Ke [b], Ling Jiang [c,d], Yuanyuan Pan [a], Ronghua Ma [a]

[a] Key Laboratory of Watershed Geographic Sciences, Nanjing Institute of Geography and Limnology, Chinese Academy of Sciences, Nanjing 210008, China
[b] School of Earth Sciences and Engineering, Hohai University, Nanjing 211100, China
[c] Anhui Center for Collaborative Innovation in Geographical Information Integration and Application, Chuzhou University, Chuzhou 239000, China
[d] School of Architecture, Building and Civil Engineering, Loughborough University, Loughborough LE11 3TU, UK

ARTICLE INFO

Article history:
Received 15 August 2018
Received in revised form 25 March 2019
Accepted 11 April 2019
Available online 13 April 2019

Keywords:
Digital elevation model
Accuracy assessment
High Mountain Asia
ICESat

ABSTRACT

Over the past decades, climate change has exerted pronounced influences on the cryo-hydrologic environments in High Mountain Asia (HMA). Digital elevation models (DEMs) are one of the critical datasets required in many hydrology- and cryosphere-related studies in HMA, which include estimations of glacier mass balances and lake water storage changes and hydrological runoff modelling. Several global or near-global coverage DEMs (e.g. SRTM and ASTER missions) have been widely utilized for such studies. However, a comprehensive assessment of the quality of these DEMs, particularly over the high-relief HMA area, is still lacking. This study investigated the performances of seven public freely-accessed DEM datasets (ASTER GDEM V2, SRTM-3 V4.1 DEM, SRTM-1 DEM, AW3D30 DEM, VFP-DEM, MERIT DEM, Seamless SRTM-1 DEM) over the HMA region by referring to high-accuracy elevation data from ICESat altimetry. We also provided an additional detailed assessment for typical lake basins and extremely rugged areas in the Himalayas by using available global positioning system (GPS) measurements and gridded SETSM DEM raster data. Results show that AW3D30 exhibits the highest accuracy in HMA land areas among these datasets. The accuracy of all studied DEMs demonstrates high spatial variation, which shows the strongest relationship with slope among several topographical factors, such as elevation and aspect. Over these rugged terrains with a large slope, such as the Hengduan Mountains and Himalayas, the vertical accuracy is relatively low in all investigated DEMs. We established empirical models for fitting the relationship between DEM vertical error and mean slope, which can be used to estimate the average elevation errors for any given local or basin-scale DEM grids. In addition, this study identified regions with anomalous elevation data in each dataset caused by the imperfect void-filling processing scheme. In sum, the 3-arc-second MERIT DEM is judged to be relatively dependable for HMA which not only achieves good performances in statistical error values but also retains few void-filling anomalies. The 1-arc-second AW3D30 could be the most promising product over HMA with its high spatial resolution and accuracy, although some void-filling anomalies need to be noted in some regions.

1. Introduction

The Earth's surface topography has a major impact on geomorphic, hydrologic, and ecological processes (Wilson, 2012). Quantitative land-surface topography analyses and many geophysical studies usually rely on Digital Elevation Models (DEMs) (Evans, 2012), which are critical baseline datasets required in the extraction of land-surface topographic parameters and objects (Drăguţ and Eisank, 2011). In particular, DEM data and other forms of elevation measurements are urgently required for the High Mountain Asia (HMA) region, where environmental changes have occurred in response to global warming and climate change. Previous studies stressed the importance of high-accuracy DEMs for quantifying glacier surface elevation changes (Ke et al., 2015; Brun et al., 2017), lake water level and volume change (Fujita et al., 2008; Zhang et al., 2011; Song et al., 2013), and water balance modelling (Wang et al., 2012) over the HMA. Given that the HMA is characterized by various land cover types, large altitude range, and extremely rugged terrains, an evaluation of the quality of various DEM datasets is an important prerequisite for specific applications.

DEMs (referring to Grid-DEM) are generally created by three methods: traditional ground survey, existing historical topographic maps, and remote sensing (Nelson et al., 2009; Persendt and Gomez, 2016). The rapid development of remote sensing techniques has resulted in the considerable increase in the availability of DEMs in terms of spatial resolution, coverage, and accuracy (Rabus et al., 2003; Liu,

* Corresponding author. 73 Beijing East Road, Nanjing, China.
E-mail address: cqsong@niglas.ac.cn (C. Song).

https://doi.org/10.1016/j.geomorph.2019.04.012
0169-555X/

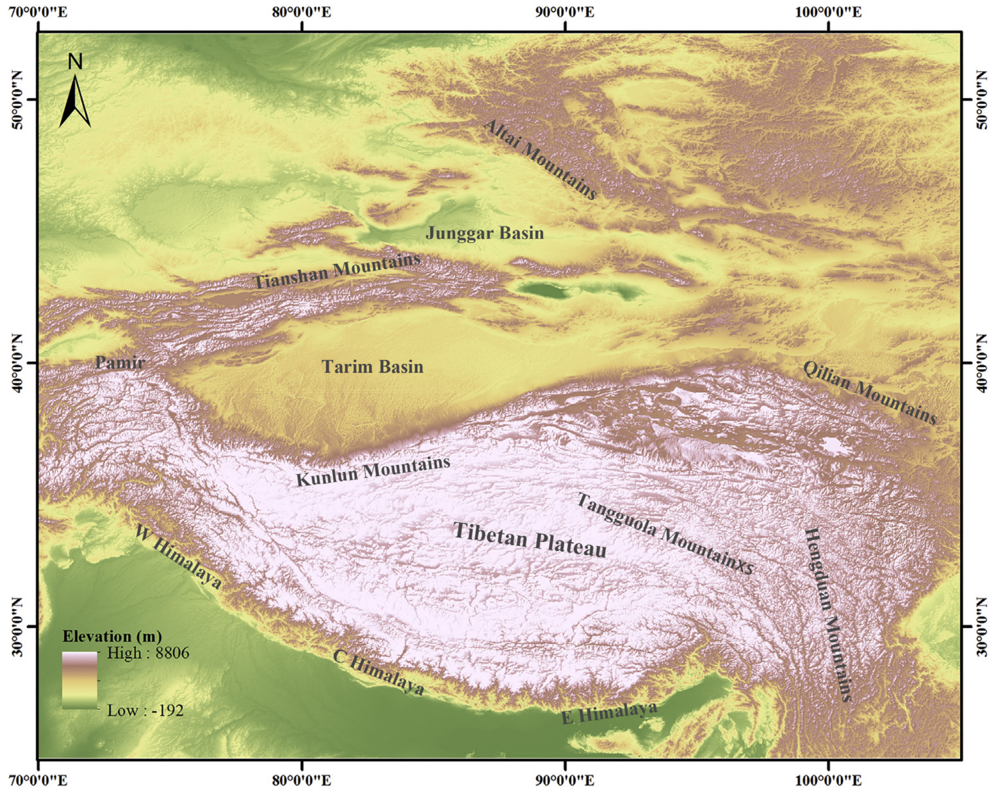

Fig. 1. Topography of HMA and the distribution of important landform units.

2008; Tarolli, 2014; Liu et al., 2016). The Shuttle Radar Topography Mission (SRTM) collected land elevations by using space-borne radar measurements on February 2000 at 1″ and 3″ resolution (referred as SRTM-1 DEM and SRTM-3 DEM, respectively). Data gaps exist the original SRTM measurements caused by the squint mode of the SAR instrument over high-relief areas (Yue et al., 2017). Thereafter, several void-free SRTM DEM products are generated by filling data voids or removing vegetation canopy errors (Yamazaki et al., 2017; Yue et al., 2017). The second source is the Reflectance Radiometer Global Digital Elevation Model (ASTER GDEM) produced by stereo-images acquired from the Advanced Spaceborne Thermal Emission from 2000 to 2008. ASTER GDEM is void-free and has a spatial resolution of approximately 30 m. The third source of global DEMs is the World 3D-30 m resolution (AW3D30) DEM, which is produced based on stereo-images acquired from the Panchromatic Remote-sensing Instrument for Stereo Mapping onboard the Advanced Land Observing Satellite (ALOS) from January 2006 to April 2011. This DEM was released by the Japan Aerospace Exploration Agency (JAXA) in 2015 (Tadono et al., 2015). DEM products from the three sources are currently the major regional DEM data for the HMA area.

When using or choosing different sources of DEM datasets in specific applications, quality assessment is a critical preliminary work. For early-stage released SRTM and ASTER GDEM, global-scale product assessments conducted by the validation teams from USGS, NASA and METI have been revealed (ASTER GDEM Validation Team, 2011; Belz et al., 2015). In addition, various local-scale accuracy assessments have been conducted in different regions (Hirt et al., 2010; Mouratidis et al., 2010; Mukherjee et al., 2013; Athmania and Achour, 2014; Satgé et al., 2015), with different land cover conditions (Zhang et al., 2016; Du et al., 2016) and different application fields (Racoviteanu et al., 2007; Wang et al., 2012). However, a comprehensive evaluation is lacking on the quality of these DEMs over the HMA region, where the topography is complex due to its rugged terrains and various landforms.

The ideal reference data for assessing DEM quality are the ground control points collected from GPS measurements. However, a wide-range field survey is time-consuming and many remote rugged places are hard to access. The Geoscience Laser Altimeter System (GLAS) onboard Ice, Cloud, and land Elevation Satellite (ICESat) provides global sampling of the land surface's height with unprecedented satellite altimetry accuracy (Zwally et al., 2002). Thus, the high-quality laser altimetry ICESat/GLAS has been used as an important reference data for evaluating DEMs, especially for large-scale studies (Bhang et al., 2007).

This study aims to conduct a systematic evaluation of the quality of global-scale, freely available DEMs over the HMA region. We collect seven sets of such DEMs, namely, ASTER GDEM V2, SRTM-3 V4.1 DEM, SRTM-1 DEM, AW3D30 DEM, VFP-DEM, MERIT DEM, and Seamless SRTM-1 DEM, and quantify their vertical accuracies by referring to elevation measurements acquired from laser altimeters onboard the

Table 1
The basic information of the adopted DEMs.

Data	Abbreviation	Spatial resolution	Acquisition technique	Data voids	Download link
ASTER GDEM V2	ASTER	1 arc-second	Satellite stereo images	None	https://earthexplorer.usgs.gov/
SRTM-3 V4.1 DEM	SRTM-3	3 arc-second	SAR Interferometry	None	https://earthexplorer.usgs.gov/
SRTM-1 DEM	SRTM-1	1 arc-second	SAR Interferometry	Yes	https://earthexplorer.usgs.gov/
AW3D30 DEM	AW3D	1 arc-second	Satellite stereo images	None	http://www.eorc.jaxa.jp/ALOS/en/aw3d30/index.htm
VFP-DEM	VFP-DEM	3 arc-second	Fusion of multisource data	None	http://viewfinderpanoramas.org/dem3.html
MERIT DEM	MERIT	3 arc-second	Fusion of multisource data	None	http://hydro.iis.u-tokyo.ac.jp/~yamadai/MERIT_DEM/
Seamless SRTM-1 DEM	SSRTM-1	1 arc-second	Fusion of multisource data	None	http://sendimage.whu.edu.cn/res/DEM_share/

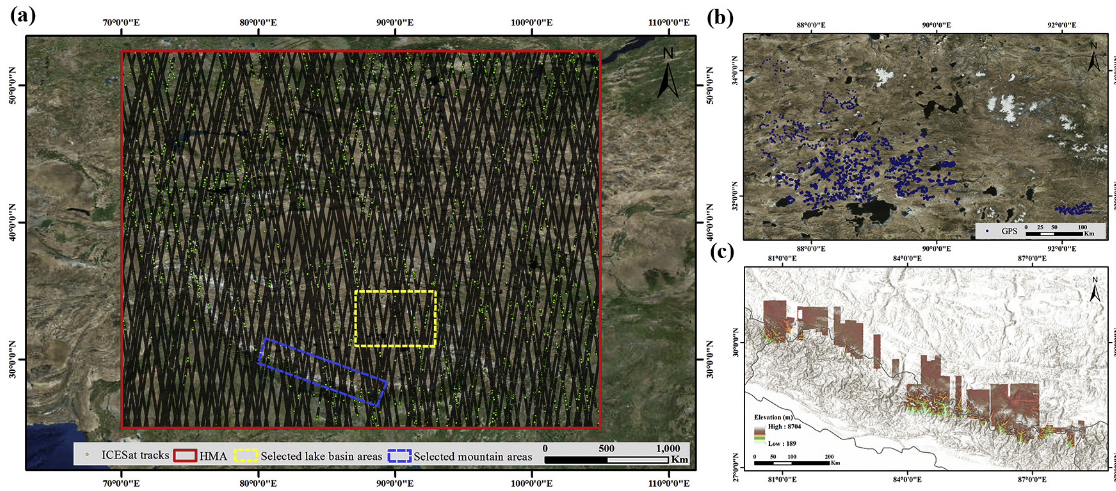

Fig. 2. Reference datasets for vertical assessments. (a) ICESat footprints in 2003 (parts of the ICESat points adopted in this paper); (b) GPS measured points in lake basin area; (c) SETSM DEM in Himalaya Mountains area.

ICESat. We also inspect specific quality issues, such as the distribution of anomalies in different datasets due to the void-filling strategy. Moreover, local-scale GPS data in the lake basins of the Changtang Plateau and 20 m resolution gridded DEM data from another source are supplemented to evaluate DEMs in the mountainous Himalayan area. The DEM assessments mainly focus on generally stable ground areas excluding lakes and glacierized areas where elevation can vary considerably in recent years. To provide guidance when using DEMs for lake- and glacier-related applications, we provide a brief discussion in the final part. Our purpose is to provide insights on the accuracy, reliability and problems in currently available DEMs over the HMA, which can help future researchers select the optimal dataset for different purposes of regional or sub-regional applications and evaluate possible uncertainties associated with the used DEM.

2. Study area and data

2.1. Study area

HMA refers to a broad mountainous area in central Asia, which consists of the Tibetan Plateau, Tarim Basin, Junggar Basin and surrounding mountains, including the Himalaya, Pamir, Tianshan, Altai, Qilian, Hengduan, Nyainqêntanglha, and Kunlun Mountains. Our studied geographic extent ranges from 25° to 52.5° N and 70° to 105°E (Fig. 1). This region is home to several different types of unique landforms and ecosystems due to the rather complex terrains and climate patterns. As the world's largest reservoir of snow and perennial glaciers except the Earth's polar ice sheet, HMA is the source of many large rivers in Asia, which feed more than a billion people along the downstream regions, such as the Yellow, Yangtze, and Ganges Rivers (Immerzeel et al., 2010). HMA poses a strong influence on the East Asian monsoon, as well as atmospheric circulations of the Northern Hemisphere because of the high altitudes and strong topographic effects (Yanai et al., 1992).

2.2. Study data

2.2.1. Global DEM datasets used in this study

In this study, seven freely available DEMs are selected, and their detailed information is listed in Table 1. ASTER GDEM V2 and SRTM-3 V4.1 are the recently updated versions, at 3-arc-second resolution, published by NASA, and have been initially processed, which involved removing extreme errors and filling data voids. In addition, two 1-arc-second second resolution DEMs, SRTM-1 and AW3D, are included. The SRTM-1 DEM has evident data voids over the HMA region.

Aside from the above mentioned four DEMs released by NASA and JAXA, three newly improved DEMs released by individual researchers are included in this study. VFP-DEM is an early improved product based on SRTM-3 that was produced by filling the data voids using alternative sources such as ASTER GDEM, digitalized paper topography maps, spot elevations on sketch maps, and Landsat images (available at http://www.viewfinderpanoramas.org/dem3.html). More recently, Yamazaki et al. (2017) released the Multi-Error-Removed Improved-Terrain DEM (MERIT DEM) at 3″ resolution after blending SRTM-3, AW3D30 and VFP-DEM using a globally consistent error removal method. In addition, in order to fill the voids in SRTM-1, Yue et al. (2017) produced seamless

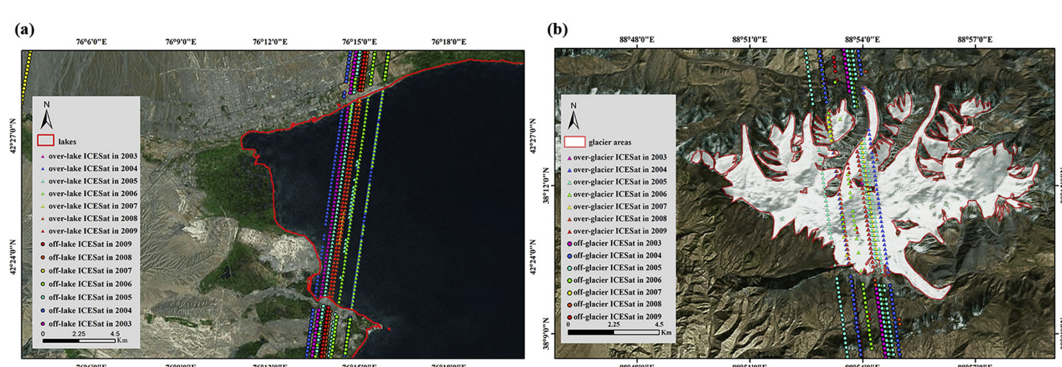

Fig. 3. Illustrations of ICESat footprints over lake areas (a) and glacier areas (b) in different years.

SRTM-1 DEM (SSRTM-1) by blending ASTER DEM and ICESat altimetry data.

2.2.2. Reference data for assessing DEM data

2.2.2.1. ICESat/GLAS altimetry data. In this study, ICESat/GLAS elevation data were used as the reference elevation data for the whole region. The primary purpose of the ICESat mission was to measure the changes in the polar ice-sheet mass and their impacts on the global sea level. The GLAS onboard ICESat produces a 1064 nm pulse for altimetry and a 532 nm pulses for the vertical distribution of clouds and aerosols (Spinhirne et al., 2005). It measures the elevation of the Earth's surface with footprints of ~70 m in diameter spaced at 170 m intervals (Kwok et al., 2004). The high accuracy of ICESat/GLAS altimetry data was reported in prior literatures and can achieve centimeter level in flat areas (Zwally et al., 2008).

We used Release-33 ICESat level-2 Global Land Surface Altimetry Data product (GLA14), which was downloaded from the National Snow and Ice Data Center (NSIDC) (http://nsidc.org/data/icesat/). A total of 28,431,016 points from 2003 to 2009 located in HMA were selected. The ICESat tracks collected in 2003 are shown in Fig. 2a to illustrate the spatial distribution of measurements.

2.2.2.2. GPS data for lake basin in the Changtang Plateau. Available GPS data are used as a supplement reference data to assess DEM performances in HMA's lake basin areas. A lake basin is a typical geomorphic unit in HMA, which is characterized by low-relief terrain. Many prior studies have focused on modelling lake water storage changes and budgets in HMA, with DEM quality in lake basin areas requiring special attention (Sheng, 2009; Song et al., 2013, 2016; Yang et al., 2017). As shown in Fig. 2b, the selected lake basin areas are located in the central Tibetan Plateau. In total, 3841 points were collected using vehicle-mounted GPS in 2012.

2.2.2.3. SETSM DEM in mountain area. Mountain area is another common geomorphic unit in HMA that deserves special focus. DEM products constructed by using side-looking SAR images, such as those based on SRTM DEM, may perform poorly over high-relief areas (refer to SRTM DEM data introduction and quality assessment literature). To fully evaluate the DEM accuracies over the mountains area, the along-track sampling of ICESat data may not be fully spatially representative. Therefore, we use a high-quality local DEM at 20 m spatial resolution (referred as SETSM DEM) as additional references. The SETSM DEM, covering the border areas between Nepal and China (Fig. 2c), was created by using the Surface Extraction with Triangulated Irregular Network-based Search-space Minimization (SETSM) algorithm based on stereo-mode satellite imagery from WorldView-1 and WorldView-2 satellites (Noh and Howat, 2015). This DEM was provided by the Polar Geospatial Center, The Ohio State University.

3. Methods

3.1. Data processing

After downloading all tiles of pieced DEMs over HMA, mosaic processing was conducted to generate the final seven HMA DEMs. The ICESat/GLA14 land surface elevation data are referenced to the Topex/Poseidon ellipsoid and EGM 2008 Geoid, which are different from the seven DEMs with the WGS84/EGM96 reference system. Thus, elevation conversion is needed by using Eq. (1).

$$ICESat\_ele = ICEsat\_eleMeasured - ICESat\_geoid - 0.7 \quad (1)$$

where 0.7 is an offset between the Topex ellipsoid and WGS84 ellipsoid, and the EGM96-geoid undulations (ICESat_geoid) should be removed for the ellipsoidal height (ICEsat_eleMeasured) to obtain the orthometric heights which are consistent with the seven DEMs (Bhang et al., 2007).

Lakes and glaciers over the HMA have experienced obvious changes in elevation with time. Therefore, we masked them out in our evaluation of the DEM products by using global lake inventory (Sheng et al., 2016) and the second Chinese glacier inventory (Guo et al., 2015). As shown in Fig. 3, the ICESat footprints over land areas and lake or glacial areas were separated with 300-m buffers of inventory data.

3.2. Vertical accuracy assessment

Point-based elevation measurements such as ICESat/GLAS data and GPS show generally higher accuracy than gridded DEM data and can therefore be regarded as ground-truth points. We extracted elevation values from the seven DEM products at the location of each ICESat/GPS measurement by using bilinear interpolation, and then compared the difference between DEM elevation and ICESat/GPS estimates by using three metrics, i.e. mean absolute error (MAE), root mean square error (RMSE), and standard deviation (STD) (Eqs. (2)–(4)).

$$MAE = \frac{\sum_{i=1}^{n} |(x_i - y_i)|}{n} \quad (2)$$

$$RMSE = \sqrt{\frac{\sum_{i=1}^{n} \left[(x_i - y_i)^2\right]}{n}} \quad (3)$$

$$STD = \sqrt{\frac{1}{n-1} \sum_{i=1}^{n} [(x_i - y_i) - (\overline{x-y})]^2} \quad (4)$$

where n is the numbers of points; x is the DEM value and y is the reference data.

4. Analyses and results

4.1. Accuracy assessment for the entire HMA based on ICESat/GLAS

4.1.1. Overall accuracy analysis based on ICESat/GLAS

The vertical accuracy assessments for void and non-void areas are conducted separately because data voids still exist in SRTM-1. As for void areas, the seamless SRTM-1 produced by Yue et al. (2017) was used to replace the invalid values in SRTM-1. The accuracy statistics are shown in Tables 2 and 3. In void-free areas, MAE, RMSE, and STD show similar variations among different datasets. Among the six datasets, the ASTER DEM (~30 m spatial resolution) has the lowest accuracy with the highest MAE (9.13 m) and RMSE (14.29 m), whereas AW3D DEM (~30 m spatial resolution) has the highest quality with

Table 2
The accuracy statistics based on ICESat in land non-void areas (units in meters).

	ASTER	SRTM-1	AW3D	SRTM-3	VFP-DEM	MERIT
Mean	0.20	0.11	0.34	0.08	0.16	0.71
MAE	9.13	3.50	2.79	4.04	3.82	3.60
RMSE	14.29	8.01	6.84	9.51	8.72	8.60
STD	14.29	8.01	6.83	9.50	8.72	8.57

Table 3
The accuracy statistics based on ICESat in land void areas (units in meters).

	ASTER	SRTM-1	AW3D	SRTM-3	VFP-DEM	MERIT
Mean	11.28	5.62	4.53	−3.87	4.57	3.64
MAE	26.92	25.21	11.89	43.52	35.43	35.05
RMSE	40.83	39.71	25.00	61.99	53.39	53.10
STD	39.25	39.31	24.59	61.87	53.19	52.98

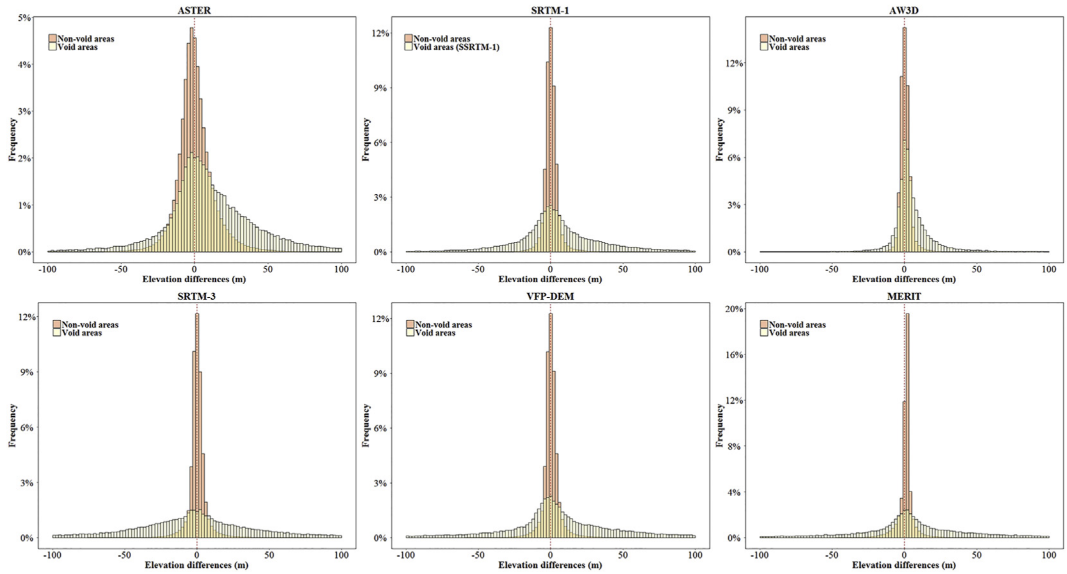

Fig. 4. Histograms of the elevation differences between DEMs and ICESat measurements in void and non-void areas.

the lowest MAE (2.79 m) and RMSE (6.84 m). At the spatial resolution of ~90 m, the best quality dataset is the MERIT DEM with MAE of 3.50 m and RMSE of 8.60 m. Both VFP-DEM and MERIT DEM show higher accuracy than the original SRTM-3, confirming their improved qualities. At the spatial resolution of ~30 m, both SRTM-1 DEM and AW3D show increased accuracy than the three 90 m resolution DEM datasets; whereas the ASTER GDEM shows degraded qualities than the SRTM-3 90 m resolution DEMs. Over the void areas, the vertical accuracy of each DEM dataset is generally much lower than that over void-free areas, partly because the void areas tend to be present in steep slopes and complex terrains. Over these void areas, DEM datasets at the spatial resolution of 20–30 m show considerably higher accuracy than the 90 m resolution SRTM-3 serial products. This result could be partly attributed to the advantages of higher resolution DEM in depicting terrain details. In summary, the AW3D demonstrates the highest accuracy in both void and non-void areas, indicating that this dataset is the most accurate regional DEM in HMA.

To reveal the pattern of elevation errors, histograms of the elevation differences between DEMs and ICESat/GLAS are presented in Fig. 4. We overlaid the histograms of void and non-void areas in combined plots for better comparative analysis. Evidently, all the datasets in non-void areas closely follow a normal distribution with a small positive bias and large positive kurtosis. Most of the footprints in void-free areas fall within a bias of ±50 m. By contrast, the histograms of elevation errors in void areas have considerably smaller kurtosis than the standard normal distribution, indicating that more elevation errors deviate away from the mean error. Note that the histograms for ASTER and AW3D in void areas have positive skewness, which means that the terrain elevations in these DEMs tend to be overestimated over the void areas.

4.1.2. Vertical accuracy vs elevation

We further investigated whether the vertical accuracy is correlated with elevation. For these statistics, all the error measurements (elevation difference between ICESat and DEMs) are divided into 11 groups

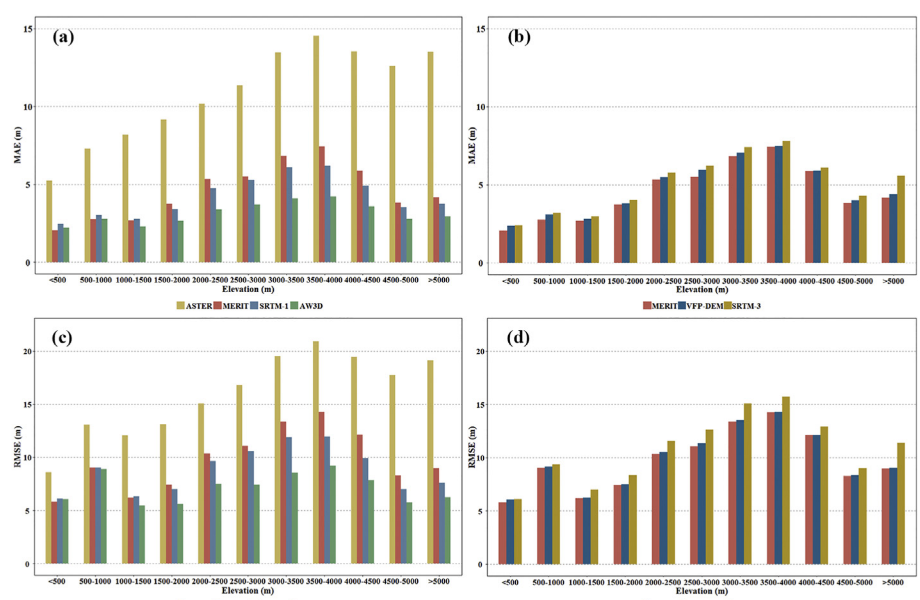

Fig. 5. The accuracy statistics in different elevation ranges. (a) MAE values among different datasets; (b) MAE values among SRTM-3 serial products; (c) RMSE values among different datasets; (d) RMSE values among SRTM-3 serial products.

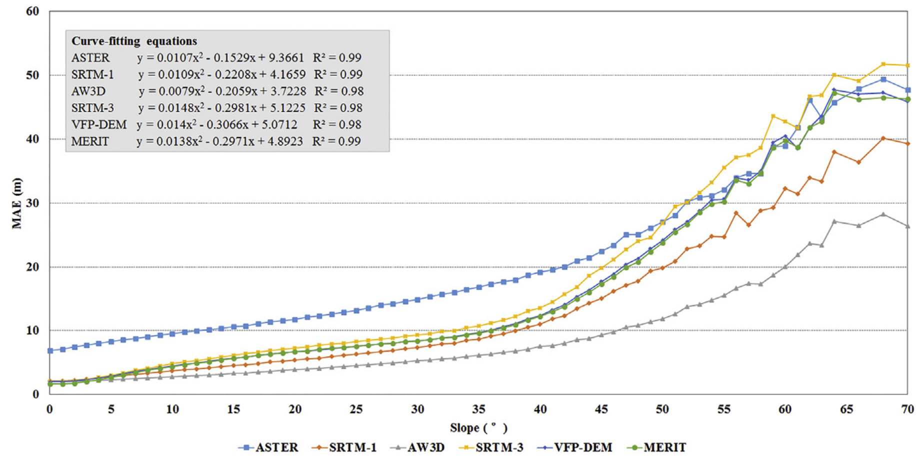

Fig. 6. The statistical relationship and empirical formulas between elevation MAE and surface slope of different examined DEMs.

at 500 m intervals, then MAE and RMSE are calculated for each elevation range (Fig. 5). Four representative DEMs from different sources and at different resolutions are selected in this analysis: ASTER, MERIT, SRTM-1, and AW3D. SRTM-3 and VFP-DEM are not chosen because they belong to the same series of products from SRTM mission at 90 m resolution and have lower accuracy than MERIT according to the analysis in the previous section.

Fig. 5 shows that both MAE and RMSE exhibit general upward trends when the elevation is lower than 4000 m, whereas the magnitudes of the errors decrease over the elevation range of 3500 m–5000 m. Note that the mean elevation errors increase when the elevation goes beyond 5000 m. Such changeover pattern can be explained by the terrain characteristics in different elevation ranges. The highest accuracy appears in the region where the elevation is <500 m, and the lowest accuracy appears at the 3500 m–4000 m elevation range. The low-altitude area is mainly distributed in the Gangetic Plain and Turpan Basin, where terrain relief is very low, whereas the high-altitude area is located along the Hengduan Mountains, where the extreme rugged topography exerts a strong influence on the DEM accuracy.

It is obvious that ASTER yields the largest errors in all the elevation ranges among the seven datasets. As for the areas where the elevation is <500 m in HMA, MERIT shows the best performance. However, the error of MERIT increases remarkably with the increase in elevation. Overall, AW3D achieves the highest accuracy in the main HMA region where elevation goes above 1500 m. A comparison among 90 m SRTM serial products is also showed in Fig. 5b and Fig. 5d. It is clear that the errors of MERIT in all elevation ranges are the smallest followed by VFP-DEM, thereby providing that the two improved DEMs enhance data quality successfully compared with the original SRTM-3.

4.1.3. Vertical accuracy vs slope

Terrain relief is widely acknowledged as a major factor in the vertical accuracy of DEMs (Jing et al., 2014). Here we present the relationship between MAE and slope, as shown in Fig. 6. All the datasets show obvious increasing trends with the increase in slope. AW3D DEM, with the lowest MAE at different slopes, evidently achieves the best performance among all the datasets, followed by SRTM-1. The advantages of AW3D and SRTM-1 are more notable with the increase in the slope value. The MAE of ASTER is obviously higher than that of any other datasets when the slope value is <50°, and then becomes lower than that of SRTM-3, VFP-DEM, and MERIT in steep areas (slope > 60°). This phenomenon is probably caused by different spatial resolutions. As for the rugged areas, the 3-arc-second DEM is not fine enough for describing the terrain relief, whereas 1-arc-second DEM has more potentials for accurate modelling of the land surface. To quantify DEM errors based on slope estimates, the second-order polynomial function was used to fit the statistical relationship between DEM errors and slope, as shown in Fig. 6. The R^2 of statistical models for all the DEM datasets are over 0.98, which enables a statistically reliable estimate of DEM errors based on mean slopes in certain areas or basins of HMA.

4.1.4. Vertical accuracy vs landform types

The possible correlation between landform types and vertical accuracy is analyzed by referring to the 1:1,000,000 geomorphologic atlas of China which was downloaded from the National Earth System Science Data Sharing Infrastructure (www.geodata.cn). This dataset has seven hierarchical layers, and the basic morphological layer is selected, which consists of two indexes: altitude and relief amplitude (Cheng et al., 2011). This atlas defines 25 types of landforms in China. Table 4

Table 4
Basic morphological types of land geomorphology in China (Cheng et al., 2011).

Altitude/relief	Low altitude <1000 m	Middle altitude 1000–3500 m	High altitude 3500–5000 m	Highest altitude >5000 m
Plain (<30 m)	Low altitude plain	Middle altitude plain	High altitude plain	Highest altitude plain
Platform (>30 m)	Low altitude platform	Middle altitude platform	High altitude platform	Highest altitude platform
Hill (<200 m)	Low altitude hill	Middle altitude hill	High altitude hill	Highest altitude hill
Low-relief mountain (200–500 m)	Low relief low altitude mountain	Low-relief middle altitude mountain	Low-relief high altitude mountain	Low-relief highest altitude mountain
Middle-relief mountain (500–1000 m)	Middle relief low altitude mountain	Middle-relief middle altitude mountain	Middle-relief high altitude mountain	Middle-relief highest altitude mountain
High-relief mountain (1000–2500 m)	–	High-relief middle altitude mountain	High-relief high altitude mountain	High-relief highest altitude mountain
Highest-relief mountain (>2500 m)	–	–	Highest-relief high altitude mountain	Highest-relief highest altitude mountain

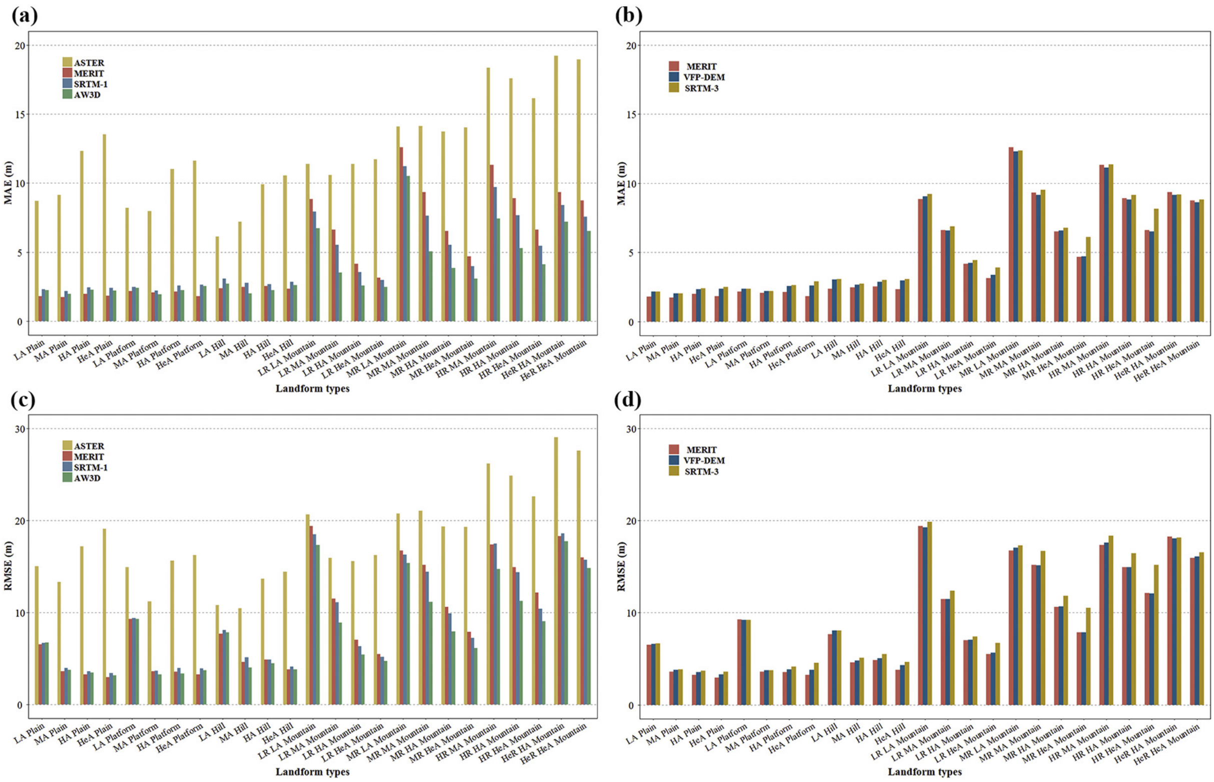

Fig. 7. The relationship between DEM measurement errors and landform types. (a) MAE values among different datasets; (b) MAE values among SRTM-3 serial products; (c) RMSE values among different datasets; (d) RMSE values among SRTM-3 serial products. (LA: low altitude; MA: middle altitude; HA: high altitude; HeA: highest altitude; LR: low relief; MR: middle relief; HR: high relief; HeR: highest relief).

summaries the classification criteria. Note that the geomorphologic database adopted in this study covers only the Chinese territory.

Fig. 7 shows the statistics of MAE and RMSE over different landforms for each selected dataset. As for plain, platform and hill areas, the MAE values for MERIT, SRTM-1, and AW3D remains stable at low levels, whereas the RMSE values in low-altitude areas are remarkably higher, thereby reflecting the great variances in the individual errors. Notably, the MAE for MERIT, SRTM-1, and AW3D in mountain regions are sensitive to the altitudes. The error in low-altitude mountain areas is much higher than that in high-altitude mountain areas, which can be explained by the distribution of more forests and artificial buildings in low or middle altitudes, thereby affecting the overall accuracy.

4.2. Accuracy assessment in the lake basin areas based on GPS

Table 5 summaries the statistical value of accuracy assessment in the lake basin areas. An obvious negative bias (approximately 2.5 m on average) exists between GPS and DEM elevations in this region, which is largely because the vehicle-mounted GPS has an initial height. GPS measurements further confirm that ASTER DEM has the lowest accuracy among the six DEMs. Except for the ASTER data, the performances of other datasets are at a similar level. AW3D has a slight advantage with the lowest values of the three statistical indicators. Notably, VFP-DEM has the same values with SRTM-3 overall, which indicates that VFP-DEM did not improve in this area.

4.3. Accuracy assessment in the Himalayan region based on SETSM DEM

Random sampling strategy based on SETSM DEM is regarded as an important supplement to test the performances in mountains areas. In total, 8674 points were created within the non-voids areas. The accuracy statistics based on the sampling points are shown in Table 6. The mean biases values for all the datasets are positive, indicating that the elevations are overestimated compared with the SETSM DEM. This finding is similar to the validations with ICESat data. Differences between SRTM-1 and SETDM DEM are the smallest, followed by AW3D. The MAE of ASTER is the highest among all the datasets. However, the RMSE of ASTER is smaller than that of SRTM-3. This phenomenon occurs because the accuracy of SRTM-3 tends to be more influenced by abnormal values. However, the absolute vertical accuracy assessments cannot be conducted due to the limited resolution of SETSM DEM.

4.4. Spatial distributions of DEM errors in HMA

The vertical assessments of the seven DEM datasets have been fully discussed in terms of statistical distributions. However, the error distributions in spatial patterns have yet to be revealed. A drainage basin is

Table 5
The accuracy statistics based on GPS in lake basin areas (units in meters).

	ASTER	SRTM-1	AW3D	SRTM-3	VFP-DEM	MERIT
Mean	−1.02	−2.32	−2.22	−2.32	−2.32	−3.14
MAE	13.01	5.46	5.39	5.67	5.67	5.89
RMSE	17.68	8.97	8.82	9.77	9.77	9.99
STD	17.65	8.67	8.53	9.49	9.49	9.48

Table 6
The accuracy statistics based on SETSM DEM (units in meters).

	ASTER	SRTM-1	AW3D	SRTM-3	VFP-DEM	MERIT
Mean	1.76	3.78	3.47	2.98	3.54	2.84
MAE	17.77	10.72	11.54	15.09	12.46	12.52
RMSE	27.85	22.91	23.33	28.22	25.23	24.90
STD	27.80	22.77	23.11	28.15	25.16	24.78

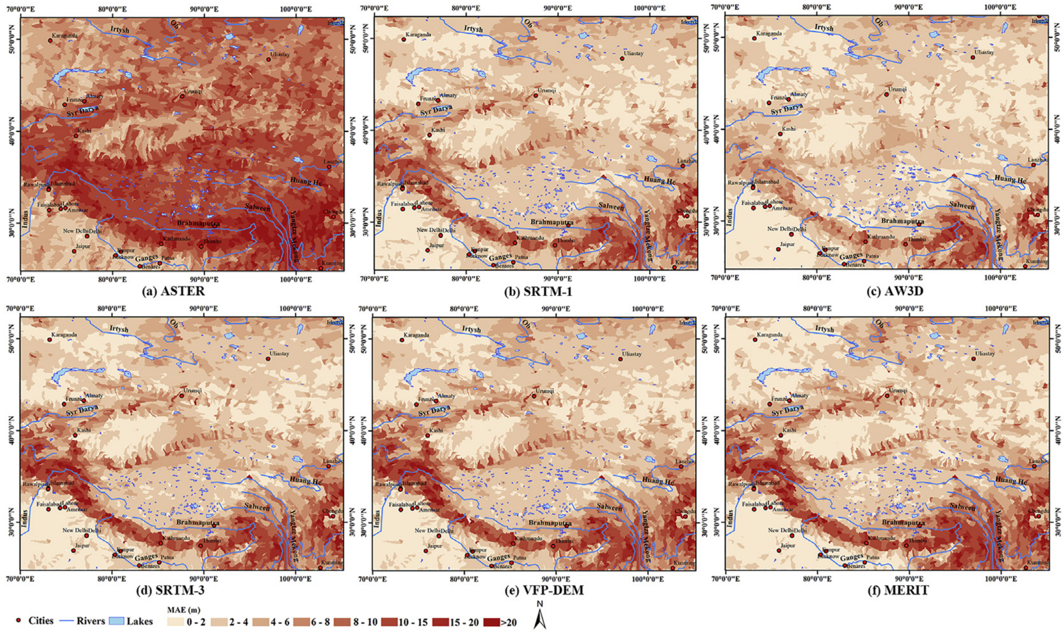

Fig. 8. Spatial distribution of basin-scale vertical error of different DEMs compared to ICESat measurements in HMA. (Note: SSRTM-1 was used in void areas to replace the invalid value in SRTM-1).

the basic unit considered in geomorphology, hydrology, and ecology with a hierarchical pattern controlled by the size of a catchment area. Each drainage basin is separated topographically from adjacent basins, thereby making it suitable as the statistical unit for topographic-related studies, especially at a macro scale (Xiong et al., 2016a). In this study, the drainage basins covering HMA are obtained from the Global Drainage Basin Database (GDBD, available online at http://www.cger.nies.go.jp/db/gdbd/-gdbd_index_e.html). A total of 5139 basins in HMA are provided by GDBD, and vertical assessments are conducted for each basin.

The spatial distributions of MAE are shown in Fig. 8. To clearly present the comparison, the same classification scheme and color ramp are applied for each dataset. Evidently, ASTER has considerably higher errors in majority basins compared with other datasets. The differences are extremely large in central Tibetan Plateau, where the terrain relief is low with extensive upland planation surfaces (Fielding et al., 1994; Xiong et al., 2016b). Almost all the basins in this region achieve an MAE value >10 m based on ASTER. By contrast, MAE values are <4 m for other datasets. Except for ASTER, the error maps of other DEMs are generally similar. The high-value areas of MAE are mainly distributed in the southern mountain areas with high relief such as the Hengduan, Himalaya, and Pamir Mountains. Furthermore, the vertical accuracy remains at a high level in most basins especially in Ganges Plain, Changtang Basin and Tarim Basin. Overall, the AW3D possesses apparent advantages over other datasets, especially in HMA. As for other regions, including plains, and hills, the 3-arc-second MERIT can ensure high accuracy.

4.5. Void-filling anomaly distributions of different datasets

Void-filling anomalies could pose serious issues when using void-filled DEMs. Such errors are not fully taken into considerations in vertical

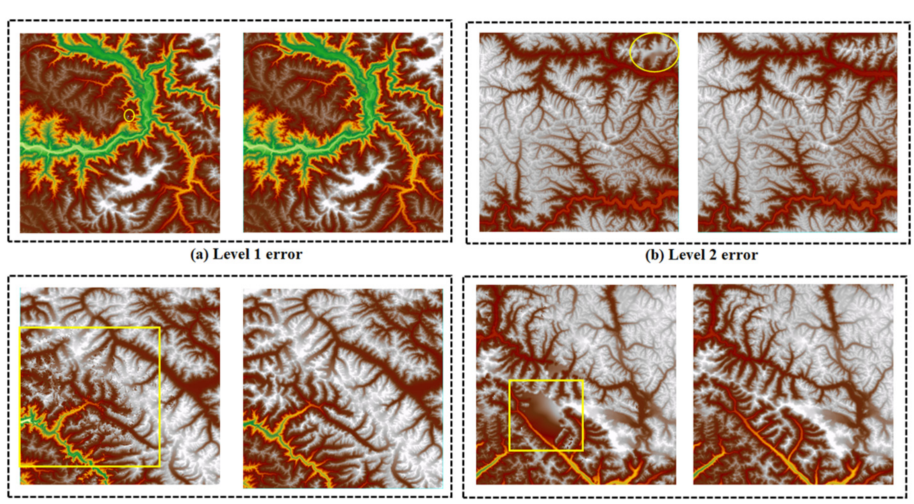

Fig. 9. Illustration of void-filling anomaly in different spatial levels according to the influence magnitudes.

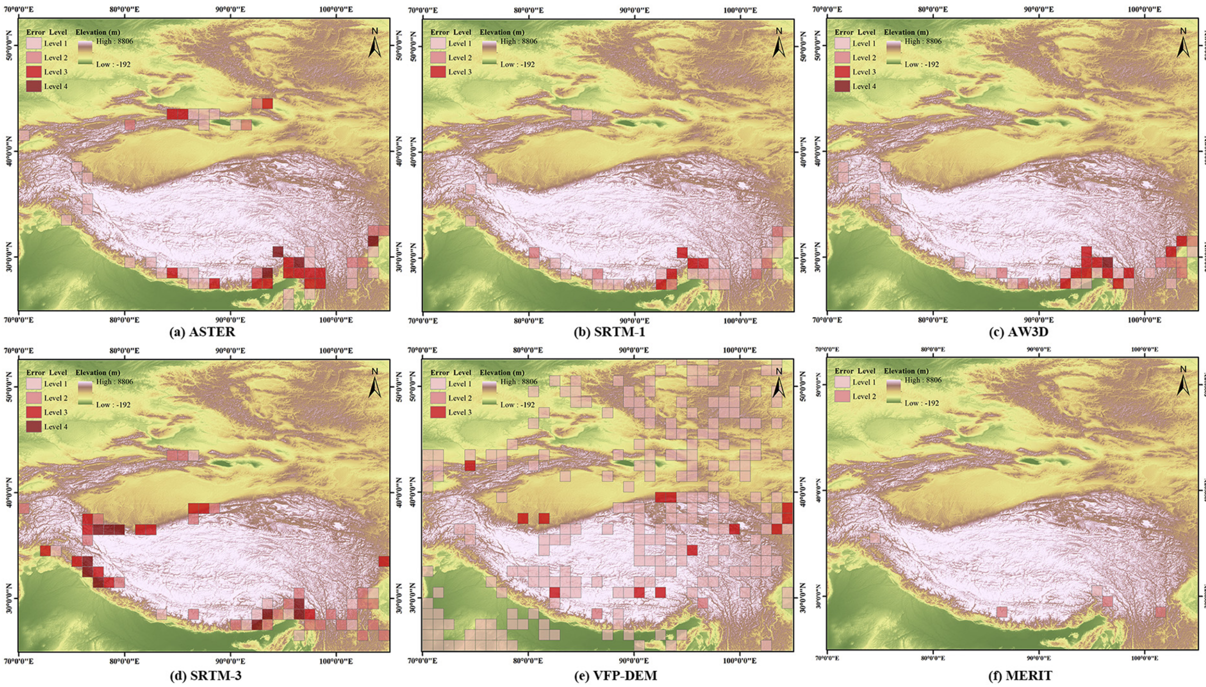

Fig. 10. The void-filling anomaly distributions of different DEMs in HMA. (Note: SSRTM-1 was used in void areas to replace the invalid value in SRTM-1.)

assessment because they are composed as gross errors. We identified such anomalies by visual interpretation and qualitatively classified them into four levels according to the level of noises. The four typical errors are shown in Fig. 9: (1) level-1 error is characterized by one or few isolated noise points or voids; (2) level-2 error is defined as a blurred region failing to describe detailed features; (3) level-3 error can be regarded as a speckle noise that covers a large range; and (4) level-4 error is described as a large anomaly area that is unusable. The assessment is conducted on 1° by 1° gridded squares on the basis of above-defined criterion. If one tile contains multiple errors, then the highest level will be assigned.

As shown in Fig. 10, the anomalies of ASTER are mainly distributed in the ridges of Hengduan Mountains and East Himalaya because the ASTER DEM employs stereo-photogrammetric DEM construction, which mainly relies on high contrast of surface textures. The lack of contrast over snow-covered and glaciated areas impairs the performance of feature-matching algorithms, resulting in lower accuracies. AW3D basically employs a similar DEM construction strategy. Hence, a similar pattern was observed. SSRTM-1 filled the voids in SRTM-1 by blending the ASTER and ICESat data, as shown in Fig. 10b. Therefore, few tiles than in AW3D and ASTER show such anomalies. SRTM-3 contains many anomalies mainly distributed in high-altitude regions (Fig. 10d). The SRTM DEM was generated by radar interferometry, which is considered inherently handicapped in mountains areas due to the disrupted in the radar backscatter in such rugged terrain. Many level 3 or 4 errors are found in SRTM-3, which restrict its applications. VFP-DEM achieves an obvious improvement in reducing level 3 errors, but still contains many level 1 errors due to pixel-scale voids (Fig. 10e). MERIT shows the best performance with the fewest elevation

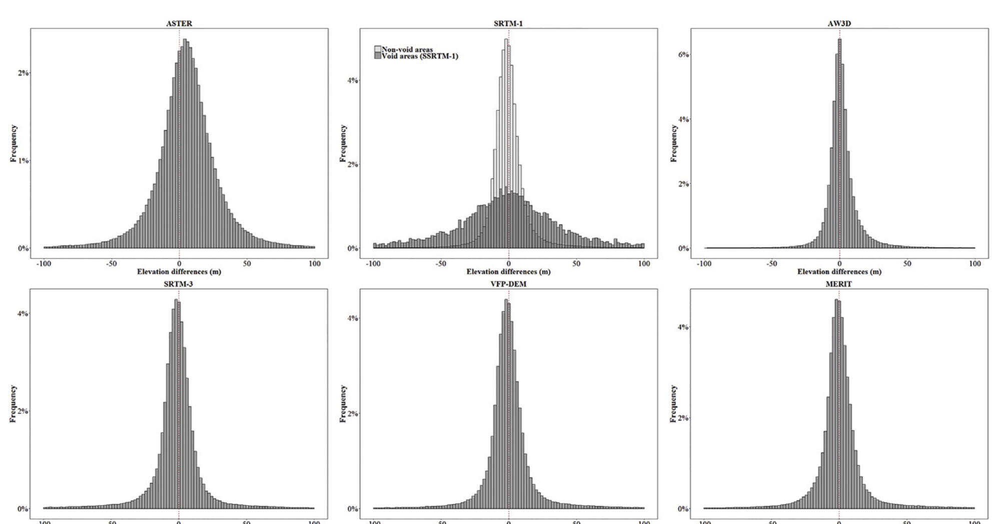

Fig. 11. Histograms of the elevation differences between DEMs and ICESat measurements in lake areas.

Table 7
The accuracy statistics based on ICESat in lake areas (units in meters).

	ASTER	SRTM-1	AW3D	SRTM-3	VFP-DEM	MERIT
Mean	−10.17	−2.44	−2.51	−2.51	−1.56	−0.89
MAE	12.00	3.23	3.25	3.25	2.59	2.90
RMSE	13.90	4.18	4.14	4.15	3.82	4.09
STD	9.47	3.39	3.29	3.30	3.49	3.99

anomalies. Only four tiles labeled as level 1 or 2 errors exist showing its great advantages over other datasets (Fig. 10f).

5. Discussion

In the above assessments, only land areas are involved without considering the lake and glacierized areas. The elevations in lake and glacier surfaces change in different years or seasons; thus, the differences in data acquisition time may cause large uncertainties in the accuracy assessment. As shown in Fig. 11 and Table 7, the differences between ICESat and ASTER, SRTM-1, SRTM-3, and VFP-DEM are considerably negative in lake areas. The negative bias can be partly explained by the lake level increase between the ICESat acquisition period (2003–2009) and the acquisition time of SRTM DEM (2000) and ASTER (2000–2008), which has been proven in previous studies (Zhang et al., 2011; Song et al., 2013, 2015a, 2015b). The acquisition year of original images obtained by ALOS for AW3D (2006 to 2009) is close to the ICESat period, which is why the elevation difference is slightly negative.

The performance of the seven datasets in glacier areas are shown in Fig. 12 and Table 8. The histograms are nearly symmetric, and only a small positive bias appears in ASTER. Melting glaciers have been found widely in HMA in the last two decades. The thinning trend of glaciers is well reflected by the negative elevation differences between ICESat and ASTER. However, such signal is not obviously presented in the differences between ICESat and SRTM serial datasets possibly because of the signal penetration offset between the radar-based SRTM and laser-based ICESat/GLAS (Rizzoli et al., 2017). The C-band of SRTM can penetrate fresh snow in glaciated areas, while ICESat/GLAS measures the surface elevation. As for the snow-covered glaciers, the elevation measured by SRTM is believed to be relatively smaller than the true surface elevation of glaciers. According to previous studies (Brun et al., 2017), the variation in thickness of glaciers from 2000 to 2006 (the median year of ICESat/GLAS data) is approximately 2–3 m, which can be offset by the penetration effect of SRTM measurements.

Table 8
The accuracy statistics based on ICESat in glacier areas (units in meters).

	ASTER	SRTM-1	AW3D	SRTM-3	VFP-DEM	MERIT
Mean	4.96	−2.75	−0.60	−0.65	0.30	1.54
MAE	18.23	13.65	9.75	9.74	12.43	7.99
RMSE	27.25	27.47	18.29	18.36	25.14	15.52
STD	26.79	27.33	18.28	18.35	25.14	15.44

6. Conclusions

This study assessed the data quality of seven commonly used and newly released DEMs covering the HMA region by referring to ICESat/GLAS altimetry data and GPS surveying points in lake basins and SETSM DEM over the Himalayan mountain regions. Excluding the lake and glacier areas, the overall vertical accuracies of each dataset were assessed in non-void and void areas. The assessment results show that AW3D achieves the highest accuracy with MAE values of 2.79 and 11.89 m over non-void and void areas, respectively, whereas the performance of ASTER is relatively poor, with MAE values of 9.13 m (non-void areas) and 26.92 m (void areas). Our analysis of the correlation between elevation, slope, and landform types and the DEM vertical accuracy shows that terrain relief exerts the strongest influences on data quality. The statistical analyses and spatial distribution maps of vertical errors indicate that DEM accuracies display obvious regional differences in HMA, with high errors in the regions of Hengduan and Himalaya Mountains.

Overall, recommendations can be given for future applications of each dataset in HMA. AW3D is the most promising dataset with high accuracy and low level of noises, however, considerable void-filling anomalies are still presented in some mountain areas. SSRTM-1 is another good choice for 1-arc-second resolution DEMs over HMA. MERIT DEM is the best choice for all available 90 m resolution DEMs for its most consistent data quality (high vertical accuracy and the fewest void-filling anomalies). Although ASTER GDEM has a comparably high spatial resolution (30 m), the assessment demonstrates that ASTER provides relatively poor elevation information in HMA except over some plain regions.

This study not only provides guidance in choosing appropriate DEMs for different kinds of geographical and geophysical studies in HMA, but also offers indications of data qualities for other regions because the HMA region represents a variety of terrains and landforms. The assessments are also beneficial in understanding the characteristics of DEMs constructed by using different remote sensing techniques. Further studies will be conducted to explore a strategy of generating improved DEMs by synthesizing these different DEM datasets.

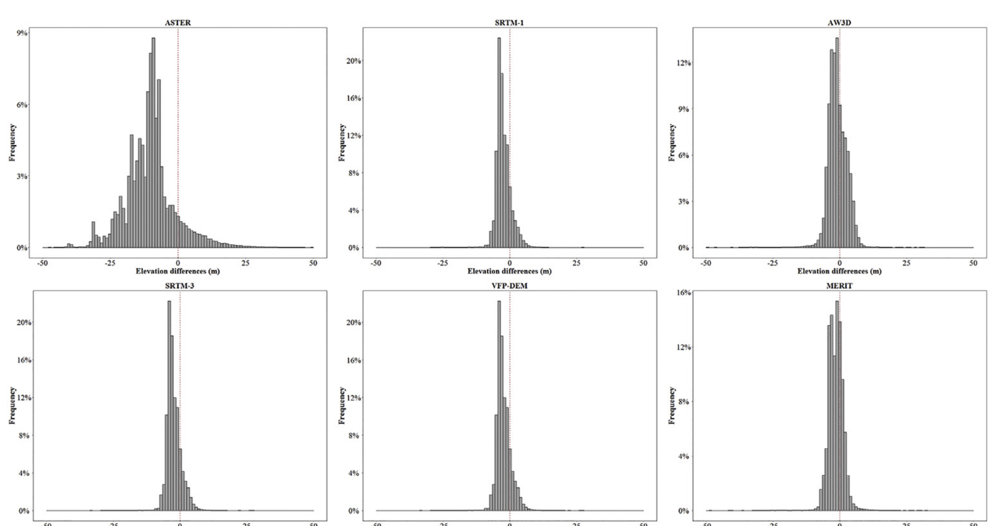

Fig. 12. Histograms of the elevation differences between DEMs and ICESat measurements in glacier areas.

Acknowledgments

This work was partly funded by the Strategic Priority Research Program of the Chinese Academy of Sciences (Grant No. XDA23100102), National Natural Science Foundation of China (No. 41801321), the National Key Research and Development Program of China (Grant No. 2018YFD0900804, 2018YFD1100101), the Thousand Young Talents Program in China (Grant No. Y7QR011001), Natural Science Foundation of Jiangsu Province of China (No. BK20161118), China Postdoctoral Science Foundation (No. 2018M642146), Jiangsu Planned Projects for Postdoctoral Research Funds (No. 2018K144C), Anhui Overseas Visiting Projects for Outstanding Young Talents in Colleges and Universities (No. gxgwfx2018078), and Nanjing Institute of Geography and Limnology, Chinese Academy of Sciences (NIGLAS2016TD01, NIGLAS2017QD15). The authors express their gratitude to the data support from National Snow and Ice Data Center, NASA, JAXA, and Lake-Watershed Science Data Center, National Earth System Science Data Sharing Infrastructure, National Science & Technology Infrastructure of China (http://lake.geodata.cn). Many thanks are also given to Dr. Lingwei Yue for providing newly processed DEMs data for this work.

References

ASTER GDEM Validation Team, 2011. ASTER Global Digital Elevation Model Version 2 Summary Report. Accessed January 15, 2018. http://www.jspacesystems.or.jp/ersdac/GDEM/ver2Validation/Summary_GDEM2_validation_report_final.pdf.
Athmania, D., Achour, H., 2014. External validation of the ASTER GDEM2, GMTED2010 and CGIAR-CSI-SRTM v4. 1 free access digital elevation models (DEMs) in Tunisia and Algeria. Remote Sens. 6 (5), 4600–4620.
Belz, J.E., Rodriguez, E., Morris, C.S., 2015. A global assessment of the SRTM performance. Photogramm. Eng. Remote Sens. 72 (3), 249–260.
Bhang, K., Schwartz, F., Braun, A., 2007. Verification of the vertical error in C-band SRTM DEM using ICESat and Landsat-7, Otter Tail County, MN. IEEE Trans. Geosci. Remote Sens. 45 (1), 36–44.
Brun, F., Berthier, E., Wagnon, P., Kääb, A., Treichler, D., 2017. A spatially resolved estimate of High Mountain Asia glacier mass balances, 2000-2016. Nat. Geosci. 10 (9), 668.
Cheng, W., Zhou, C., Chai, H., Zhao, S., Liu, H., Zhou, Z., 2011. Research and compilation of the geomorphologic Atlas of the People's Republic of China (1: 1,000,000). J. Geogr. Sci. 21 (1), 89–100.
Drăguţ, L., Eisank, C., 2011. Object representations at multiple scales from digital elevation models. Geomorphology 129 (3–4), 183–189.
Du, X., Guo, H., Fan, X., Zhu, J., Yan, Z., Zhan, Q., 2016. Vertical accuracy assessment of freely available digital elevation models over low-lying coastal plains. International Journal of Digital Earth 9 (3), 252–271.
Evans, I., 2012. Geomorphometry and landform mapping: what is a landform? Geomorphology 137 (1), 94–106.
Fielding, E., Isacks, B., Barazangi, M., Duncan, C., 1994. How flat is Tibet? Geology 22 (2), 163–167.
Fujita, K., Suzuki, R., Nuimura, T., Sakai, A., 2008. Performance of ASTER and SRTM DEMs, and their potential for assessing glacial lakes in the Lunana region, Bhutan Himalaya. J. Glaciol. 54 (185), 220–228.
Guo, W., Liu, S., Xu, J., Wu, L., Shangguan, D., Yao, X., Wei, J., Bao, W., Yu, P., Liu, Q., Jiang, Z., 2015. The second Chinese glacier inventory: data, methods and results. J. Glaciol. 61 (226), 357–372.
Hirt, C., Filmer, M., Featherstone, W., 2010. Comparison and validation of the recent freely available ASTER-GDEM ver1, SRTM ver4. 1 and GEODATA DEM-9S ver3 digital elevation models over Australia. Aust. J. Earth Sci. 57 (3), 337–347.
Immerzeel, W.W., Beek, L.P.H.V., Bierkens, M.F.P., 2010. Climate change will affect the Asian water towers. Science 328 (5984), 1382–1385.
Jing, C., Shortridge, A., Lin, S., Wu, J., 2014. Comparison and validation of SRTM and ASTER GDEM for a subtropical landscape in Southeastern China. Int. J. Digit Earth. 7 (12), 969–992.
Ke, L., Ding, X., Song, C., 2015. Heterogeneous changes of glaciers over the western Kunlun Mountains based on ICESat and Landsat-8 derived glacier inventory. Remote Sens. Environ. 168, 13–23.
Kwok, R., Zwally, H.J., Yi, D., 2004. ICESat observations of Arctic sea ice: a first look. Geophys. Res. Lett. 31, L16401.
Liu, X., 2008. Airborne LiDAR for DEM generation: some critical issues. Progress in Physical Geography 32 (1), 31–49.
Liu, K., Ding, H., Tang, G., Na, J., Huang, X., Xue, Z., Yang, X., Li, F., 2016. Detection of catchment-scale gully-affected areas using unmanned aerial vehicle (UAV) on the Chinese Loess Plateau. ISPRS International Journal of Geo-Information. 5 (12), 238.
Mouratidis, A., Briole, P., Katsambalos, K., 2010. SRTM 3″ DEM (versions 1, 2, 3, 4) validation by means of extensive kinematic GPS measurements: a case study from North Greece. Int. J. Remote Sens. 31 (23), 6205–6222.
Mukherjee, S., Joshi, P.K., Mukherjee, S., Ghosh, A., Garg, R.D., Mukhopadhyayd, A., 2013. Evaluation of vertical accuracy of open source Digital Elevation Model (DEM). Int. J. Appl. Earth Obs. 21 (4), 205–217.
Nelson, A., Reuter, H.I., Gessler, P., 2009. DEM production methods and sources. In: Hengl, T., Reuter, H.I. (Eds.), Geomorphometry: Concepts, Software, and Applications. Elsevier, Amsterdam, pp. 65–85.
Noh, M.J., Howat, I.M., 2015. Automated stereo-photogrammetric DEM generation at high latitudes: Surface Extraction with TIN-based Search-space Minimization (SETSM) validation and demonstration over glaciated regions. GIScience & Remote Sensing 52 (2), 198–217.
Persendt, F.C., Gomez, C., 2016. Assessment of drainage network extractions in a low-relief area of the Cuvelai Basin (Namibia) from multiple sources: LiDAR, topographic maps, and digital aerial orthophoto graphs. Geomorphology 260 (1), 32–50.
Rabus, B., Eineder, M., Roth, A., Bamler, R., 2003. The shuttle radar topography mission—a new class of digital elevation models acquired by spaceborne radar. ISPRS J. Photogram. Remote Sens. 57 (4), 241–262.
Racoviteanu, A.E., Manley, W.F., Arnaud, Y., Williams, M.W., 2007. Evaluating digital elevation models for glaciologic applications: an example from Nevado Coropuna, Peruvian Andes. Glob. Planet. Chang. 59 (1–4), 110–125.
Rizzoli, P., Martone, M., Gonzalez, C., Wecklich, C., Tridon, D.B., Bräutigam, B., Wessel, B., 2017. Generation and performance assessment of the global TanDEM-X digital elevation model. ISPRS J. Photogramm. Remote Sens. 132, 119–139.
Satgé, F., Bonnet, M.P., Timouk, F., Calmant, S., Pillco, R., Molina, J., Garnier, J., 2015. Accuracy assessment of SRTM v4 and ASTER GDEM v2 over the Altiplano watershed using ICESat/GLAS data. Int. J. Remote Sens. 36 (2), 465–488.
Sheng, Y., 2009. Paleolaker: a semiautomated tool for regional-scale paleolake recovery using geospatial information technologies. IEEE Geosci. Rem. Sens. Lett. 6 (4), 797–801.
Sheng, Y., Song, C., Wang, J., Lyons, E.A., Knox, B.R., Cox, J.S., Gao, F., 2016. Representative lake water extent mapping at continental scales using multi-temporal landsat-8 imagery. Remote Sens. Environ. 185, 129–141.
Song, C., Huang, B., Ke, L., 2013. Modeling and analysis of lake water storage changes on the Tibetan Plateau using multi-mission satellite data. Remote Sens. Environ. 135, 25–35.
Song, C., Ye, Q., Cheng, X., 2015a. Shifts in water-level variation of Namco in the central Tibetan Plateau from ICESat and CryoSat-2 altimetry and station observations. Science bulletin 60 (14), 1287–1297.
Song, C., Ye, Q., Sheng, Y., Gong, T., 2015b. Combined ICESat and CryoSat-2 altimetry for accessing water level dynamics of Tibetan lakes over 2003–2014. Water 7 (9), 4685–4700.
Song, C., Huang, B., Ke, L., Ye, Q., 2016. Precipitation variability in High Mountain Asia from multiple datasets and implication for water balance analysis in large lake basins. Glob. Planet. Chang. 145, 20–29.
Spinhirne, J.D., Palm, S.P., Hart, W.D., Hlavka, D.L., Welton, E.J., 2005. Cloud and aerosol measurements from GLAS: overview and initial results. Geophys. Res. Lett. 322 (22), 109–127.
Tadono, T., Takaku, J., Tsutsui, K., Oda, F., Nagai, H., 2015. Status of “ALOS World 3D (AW3D)” global DSM generation. Geoscience and Remote Sensing Symposium (IGARSS), 2015 IEEE International, pp. 3822–3825.
Tarolli, P., 2014. High-resolution topography for understanding Earth surface processes: Opportunities and challenges. Geomorphology 216, 295–312.
Wang, W., Yang, X., Yao, T., 2012. Evaluation of ASTER GDEM and SRTM and their suitability in hydraulic modelling of a glacial lake outburst flood in southeast Tibet. Hydrol. Process. 26 (2), 213–225.
Wilson, J.P., 2012. Digital terrain modeling. Geomorphology 137 (1), 107–121.
Xiong, L., Tang, G., Strobl, J., Zhu, A., 2016a. Paleotopographic controls on loess deposition in the Loess Plateau of China. Earth Surf. Process. Landf. 41 (9), 1155–1168.
Xiong, L., Tang, G., Zhu, A., Qian, Y., 2016b. A peak-cluster assessment method for the identification of upland planation surfaces. Int. J. Geogr. Inf. Syst. 31 (2), 387–404.
Yamazaki, D., Ikeshima, D., Tawatari, R., Yamaguchi, T., O'Loughlin, F., Neal, J.C., Sampson, C.C., Kanse, S., Bates, P.D., 2017. A high accuracy map of global terrain elevations. Geophys. Res. Lett. 322 (22), 109–127.
Yanai, M., Li, C., Song, Z., 1992. Seasonal heating of the Tibetan Plateau and its effects on the evolution of the Asian summer monsoon. Journal of the Meteorological Society of Japan. Ser. II 70 (1B), 319–351.
Yang, R., Zhu, L., Wang, J., Ju, J., Ma, Q., Turner, F., Guo, Y., 2017. Spatiotemporal variations in volume of closed lakes on the Tibetan Plateau and their climatic responses from 1976 to 2013. Clim. Chang. 140 (3–4), 1–13.
Yue, L., Shen, H., Zhang, L., Zheng, X., Zhang, F., Yuan, Q., 2017. High-quality seamless DEM generation blending SRTM-1, ASTER GDEM v2 and ICESat/GLAS observations. ISPRS J. Photogramm. Remote Sens. 123, 20–34.
Zhang, G., Xie, H., Kang, S., Yi, D., Ackley, S.F., 2011. Monitoring lake level changes on the Tibetan Plateau using ICESat altimetry data (2003–2009). Remote Sens. Environ. 115 (7), 1733–1742.
Zhang, Q., Yang, Q., Wang, C., 2016. SRTM error distribution and its associations with landscapes across China. Photogramm. Eng. Remote Sens. 82 (2), 135–148.
Zwally, H.J., Schutz, B., Abdalati, W., Abshire, J., Bentley, C., Brenner, A., Herring, T., 2002. ICESat's laser measurements of polar ice, atmosphere, ocean, and land. J. Geodyn. 34 (3–4), 405–445.
Zwally, H.J., Yi, D.H., Kwok, R., Zhao, Y.H., 2008. ICESat measurements of sea ice freeboard and estimates of sea ice thickness in the Weddell Sea. J. Geophys. Res. Oceans 113, C02S15.